



A zone melting device for the *in situ* observation of directional solidification using high-energy synchrotron x rays

Cite as: Rev. Sci. Instrum. **91**, 093901 (2020); <https://doi.org/10.1063/5.0019020>

Submitted: 19 June 2020 . Accepted: 14 August 2020 . Published Online: 01 September 2020

C. Gombola , G. Hasemann, A. Kauffmann , I. Sprenger, S. Laube, A. Schmitt, F. Gang, V. Bolbut, M. Oehring, M. Blankenburg, N. Schell, P. Staron, F. Pyczak, M. Krüger, and M. Heilmaier

COLLECTIONS

 This paper was selected as an Editor's Pick



View Online



Export Citation



CrossMark

ARTICLES YOU MAY BE INTERESTED IN

[Characterization of the pressure coefficient of manganin and temperature evolution of pressure in piston-cylinder cells](#)

Review of Scientific Instruments **91**, 095103 (2020); <https://doi.org/10.1063/5.0022650>

[Ion beam diagnostic for the assessment of miniaturized electric propulsion systems](#)

Review of Scientific Instruments **91**, 093501 (2020); <https://doi.org/10.1063/5.0010589>

[Mie scattering revisited: Study of bichromatic Mie scattering of electromagnetic waves by a distribution of spherical particles](#)

Review of Scientific Instruments **91**, 083112 (2020); <https://doi.org/10.1063/5.0015050>



Your Qubits. Measured.

Meet the next generation of quantum analyzers

- Readout for up to 64 qubits
- Operation at up to 8.5 GHz, mixer-calibration-free
- Signal optimization with minimal latency

Find out more



A zone melting device for the *in situ* observation of directional solidification using high-energy synchrotron x rays

Cite as: Rev. Sci. Instrum. 91, 093901 (2020); doi: 10.1063/5.0019020

Submitted: 19 June 2020 • Accepted: 14 August 2020 •

Published Online: 1 September 2020



View Online



Export Citation



CrossMark

C. Gombola,¹  G. Hasemann,² A. Kauffmann,^{1,a)}  I. Sprenger,¹ S. Laube,¹ A. Schmitt,¹ F. Gang,¹ V. Bolbut,² M. Oehring,³ M. Blankenburg,³ N. Schell,³ P. Staron,³ F. Pyczak,³ M. Krüger,² and M. Heilmaier¹

AFFILIATIONS

¹Karlsruhe Institute of Technology (KIT), Institute for Applied Materials (IAM-WK), Engelbert-Arnold-Str. 4, 76131 Karlsruhe, Germany

²Otto von Guericke University, Institute for Materials and Joining Technology, Universitätsplatz 2, 39106 Magdeburg, Germany

³Helmholtz-Zentrum Geesthacht, Institute of Materials Research, Max-Planck-Str. 1, 21502 Geesthacht, Germany

^{a)}Author to whom correspondence should be addressed: alexander.kauffmann@kit.edu

ABSTRACT

Directional solidification (DS) is an established manufacturing process to produce high-performance components from metallic materials with optimized properties. Materials for demanding high-temperature applications, for instance in the energy generation and aircraft engine technology, can only be successfully produced using methods such as directional solidification. It has been applied on an industrial scale for a considerable amount of time, but advancing this method beyond the current applications is still challenging and almost exclusively limited to post-process characterization of the developed microstructures. For a knowledge-based advancement and a contribution to material innovation, *in situ* studies of the DS process are crucial using realistic sample sizes to ensure scalability of the results to industrial sizes. Therefore, a specially designed Flexible Directional Solidification (FlexiDS) device was developed for use at the P07 High Energy Materials Science beamline at PETRA III (Deutsches Elektronen-Synchrotron, Hamburg, Germany). In general, the process conditions of the crucible-free, inductively heated FlexiDS device can be varied from 6 mm/h to 12 000 mm/h (vertical withdrawal rate) and from 0 rpm to 35 rpm (axial sample rotation). Moreover, different atmospheres such as Ar, N₂, and vacuum can be used during operation. The device is designed for maximum operation temperatures of 2200 °C. This unique device allows *in situ* examination of the directional solidification process and subsequent solid-state reactions by x-ray diffraction in the transmission mode. Within this project, different structural intermetallic alloys with liquidus temperatures up to 2000 °C were studied in terms of liquid–solid regions, transformations, and decompositions, with varying process conditions.

Published under license by AIP Publishing. <https://doi.org/10.1063/5.0019020>

I. INTRODUCTION

Directional solidification has been applied on an industrial scale, mostly to nickel-based superalloys, since the 1970s.¹ Especially for high-temperature materials, used under creep conditions, directional solidification is a promising process. During processing, the established liquid region of the sample moves out of the heated zone and is subjected to the temperature gradient, and due to that single-crystalline components or components at least exhibiting an elongated microstructure perpendicular to the temperature

gradient form. These elongated microstructures can be oriented with respect to the loading direction during application of the part since transversely oriented grain boundaries are a source of creep pores. By the alignment of the microstructure, creep rupture can, therefore, be reduced or even eliminated.¹ For example, incorporating an aligned second phase (e.g., Cr or Mo) into NiAl^{2,3} improves the creep resistance along the growth direction and increases the damage tolerance by toughening. These alloys were often produced by using a Bridgman-type directional solidification apparatus, where the heated crucible rests on a water-cooled copper base. Lowering

the base with a specific rate provides a movement of the melt from the hot zone into a liquid metal bath.⁴⁻⁷ Another technique used is an optical floating zone furnace. Here, the heating source is a xenon arc-lamp emitting infrared radiation, which is focused on the specimen enclosed in a quartz tube.^{2,3,8} The authors of Refs 9 and 10 produced directionally solidified specimens in a crucible-free mode by the electromagnetically levitated zone process. A crucible-free process offers the advantage of no contamination/reaction from the crucible with the sample even at very high temperatures.

Even though directional solidification has been applied on an industrial scale, advancing this method beyond the current applications is still challenging. Moreover, the conventional casting and directional solidification processes are not suitable for all high-temperature materials beyond nickel-based superalloys. A limiting factor is a possible reaction of the material with the crucible at such elevated temperatures. Novel materials or changes in the components require significant changes in the process parameters, which is mostly done on a trial and error basis. A knowledge-based advancement of the process is difficult as—at least to some extent—there is no possibility to characterize the production process and the materials behavior “*in situ*.” So far, the process characterization was limited to post-process investigations of the evolving microstructure, which are often not the same as directly formed by cooling short below the solidus temperature.

X-ray diffraction methods are suitable for *in situ* studies of the DS process. With these techniques, the investigation of the liquid zone and solidification front is possible in the transmission mode. Due to the high temperatures and the difficulties in handling sufficient amounts of hot melt, studies of the melting and solidification behaviors so far have almost exclusively been performed for metals or alloys with rather low melting points, e.g., magnesium or gallium–indium alloys.¹¹⁻¹³ Our crucible-free, inductively heated FlexiDS device allows *in situ* studies of the synthesis, transformation, and decomposition of various structural intermetallic materials with maximum liquidus temperatures of 2200 °C via diffraction of high-energy synchrotron radiation. The maximum sample diameter is 14 mm, which is a compromise between possible x-ray transmission and a process that is close enough to relevant industrial processes concerning temperature distribution in the solid and convection in the melt. The device has been designed for the use at the P07 High Energy Materials Science (HEMS) beamline at PETRA III [Deutsches Elektronen-Synchrotron (DESY), Hamburg, Germany], where the combination of a high photon flux ($>10^{12}$ 1/s) and fast readout 2D detectors (15 Hz) enables the study of this complex liquid–solid interactions during solidification and subsequent solid-state reactions. The available detectors cover a range up to 250 Hz, corresponding to a temporal resolution of 4 ms. However, 250 Hz is never needed with thick samples. The high beam energy of typically 100 keV allows transmission of samples with various diameters (14 mm–8 mm) and densities typically between the TiAl and Mo-based alloys. A large portion of reciprocal space can be investigated at rapid acquisition times (typically 1 s–30 s, depending on the sample size and alloy system). This technical environment enables us to investigate the local evolution of the microstructure during directional growth depending on different process conditions (withdrawal rate, rotation speed, and rod diameter).

In the following, the directional solidification device and its use for characterizing the processes occurring during solidification are

described in detail. This provides the base for an understanding of solidification and the development of alloys, which are produced by directional solidification.

II. TECHNICAL LAYOUT OF THE FLEXIDS DEVICE

The DS device is, in essence, independent and can, thus, be used either in the laboratory or it can be integrated at a beamline [here, the P07 High Energy Materials Science (HEMS) beamline at PETRA III]. In order to perform *in situ* investigations during directional solidification with the required flexibility, the device has to fulfill both the requirements of the directional solidification process and the additional demands for combining this process technology with x-ray diffraction geometries.

A schematic drawing of the main modules of the device is visualized in Fig. 1. The mechanical setup manufactured by SYSTEC Fertigungstechnik GmbH & Co. KG¹⁴ includes the following modules: (I) the directional solidification device on a positioning stage, (II) the energy supply and vacuum pump, and (III) the water battery (Fig. 1). All components are designed for a flexible setup and transport. Therefore, a precise positioning of the chamber with respect to the x-ray beam is possible. For the directional solidification process, a clean and protective atmosphere is essential to protect the material from oxidation and contamination. For the sake of clarity, Fig. 2 gives an overview of the complex device with all components and features. Important features and parameters are compiled in the following list:

- Atmosphere: Ar, N₂, and vacuum
- Heating: inductive
- Power: 12 kW (150 kHz–375 kHz)
- T_{max}: 2200 °C (tested 2000 °C)

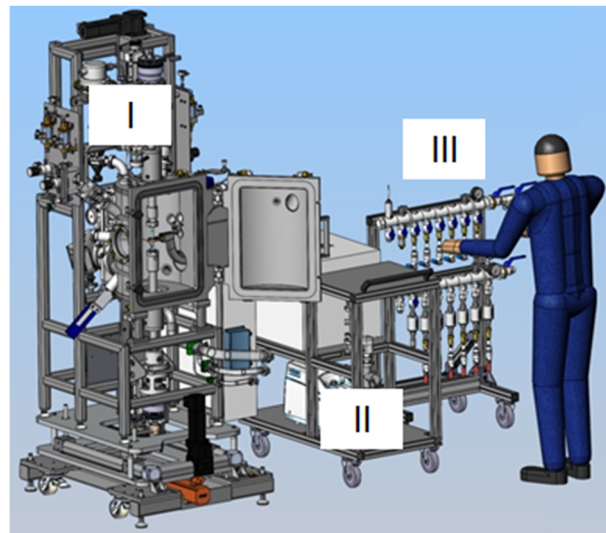


FIG. 1. Schematic of the modules of the setup: (I) the directional solidification device on a positioning stage, (II) the energy supply and vacuum pump, and (III) the water battery. The person is displayed here to estimate the size and usability of the device.

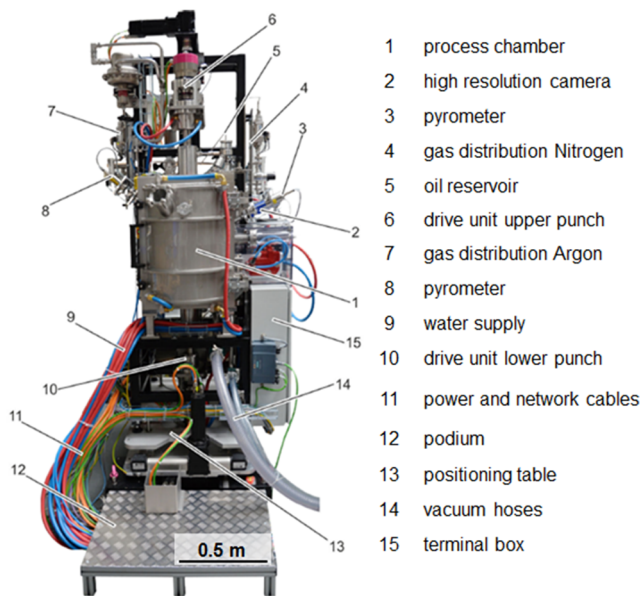


FIG. 2. Overview of the zone melting device with its components.

- Rod-shaped samples from 8 mm to 14 mm in diameter
- Vertical withdrawal rate: 6 mm/h–12 000 mm/h (6 mm/h increments, tested so far 6 mm/h–360 mm/h)
- Axial sample rotation: 0 rpm–35 rpm (1 rpm steps), synchronous rotation, or counter rotation
- Temperature observation: two pyrometers positioned at the liquid zone (in the coil) and 10 mm above

The manually controlled power of 12 kW is spread from 0% to 100% and can be adjusted in 0.1% steps, which enables the user to reach and maintain the sample in the liquid state.

A. Process chamber

A visual inspection of the process chamber interior is possible via multiple windows and a lamp illuminating the chamber. Furthermore, the process chamber can be monitored via two high-resolution cameras suitable for high temperature image acquisition (detailed description in Sec. III). These cameras may also be used to observe the liquid zone of the sample. Two pyrometers detect the temperature of the rod inside the coil and at an adjustable distance above the coil (typically 10 mm above the induction coil). With this arrangement, the temperature can be measured in the liquid zone and at 10 mm distance, usually already in the solid state of the sample. With the assumption of a linear temperature decrease, a temperature gradient can be determined. The temperature evolution plays an important role in terms of process control and power adjustment. Spare flanges can be used for additional measuring devices or other attachments. One is located at the chamber door (DN 25 ISO-KF) (Fig. 2) and a second at the backside of the chamber (DN 40 ISO-KF) (Fig. 3). Figure 3 shows the interior view of the chamber. For the sake of safety and sealing, the process chamber door is equipped with two locks. Moreover, a door protection switch is attached, which

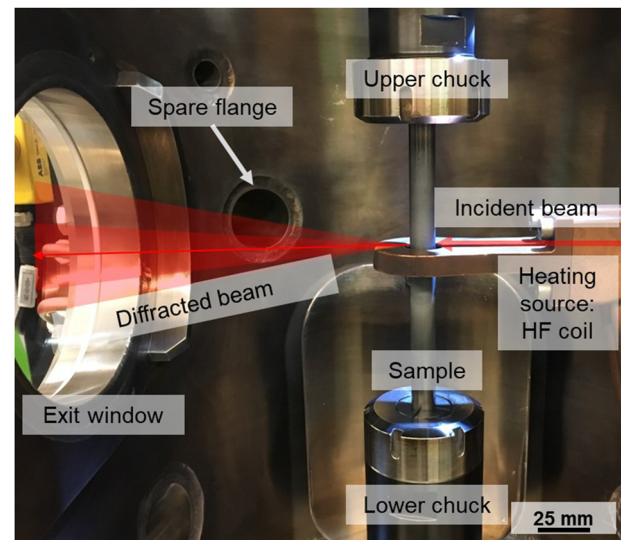


FIG. 3. Interior of the process chamber: the water-cooled chucks and the high frequency (HF) coil as the heating source are highlighted. The x-ray beam enters the chamber on the right side and interacts with the sample, and the diffracted beam leaves the chamber on the left side through the larger window.

prevents that process gas flow, and heating is activated if the process chamber door is open.

B. Sample holder and induction coil

The sample passes through the induction coil (Fig. 3) and is fixed in the upper and lower drive shafts by clamping jaws. 10 mm of the sample is needed on both ends for mounting the sample on the clamping system. Together with a typical safety distance of 20 mm from the coil below and above preventing induction in the clamps, the sample length is calculated. The upper chuck is tightened manually, while the lower one has a pneumatic system in order to allow the sample to expand during heating up and tighten it right before the liquid zone forms. With the two independent drive shafts, a vertical movement of the sample and synchronous or counter rotation can be applied. The induction coil displayed schematically in Fig. 4(a) was specially designed for *in situ* experiments and is suitable for the above-mentioned sample geometries. An integrated water circuit achieves cooling of the coil, chucks, and housing. The conical recess in the coil prevents cutting off for the diffracted beam to pass [Fig. 4(a)]. Figure 4(b) gives an insight into the chamber during heating. For the *in situ* experiments, the samples were usually moved upward (lifted) through the coil due to the position of the beam and the recess of the coil. Thus, the upper sample part represents the directionally solidified part, and the lower part is called the feed, which is in the as-cast condition. For the results shown in Sec. V, both parts of the rod are rotated with the same speed and direction, but these two parameters can also be varied independently.

C. Positioning stage

In order to move the FlexiDS process chamber with respect to the incident beam parallel as well as transverse to the samples'

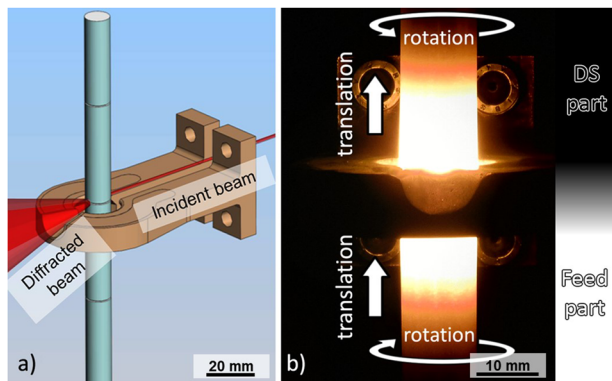


FIG. 4. (a) Detail of the specifically designed HF coil and (b) HF coil and a heated sample during processing. Arrows indicate the process movement in terms of the withdrawal rate and rotation speed.

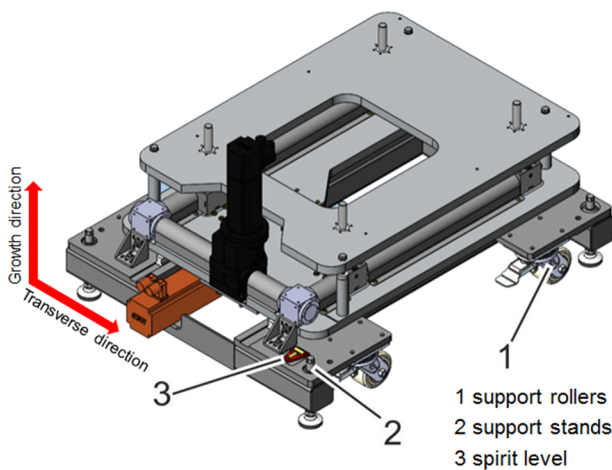


FIG. 5. Positioning stage: the range of motion is ± 50 mm parallel and transverse to the growth direction.

growth direction, the system is mounted on a positioning stage (Fig. 5). Once placed with support rollers at the final position, the device is set on the support stands, which are located at the corners of the stage. A spirit level facilitates the adjustment and ensures the horizontal alignment. The movement range is ± 50 mm in the growth direction and transverse to the growth direction. The smallest positioning increment is 0.05 mm, allowing an accurate positioning with respect to the incoming beam.

III. WORKSTATIONS AND CONTROL SOFTWARE

Two workstations, a mobile panel and a PC workstation, are connected to the device. The control software is implemented by ITG induction systems.¹⁵ Generally, two modes of operation are possible: “manual mode,” mainly operating the mobile panel, and “auto mode,” mainly suited for the PC control during *in situ* experiments.

The mobile panel next to the chamber allows fast and precise setting up and positioning of the sample. In order to achieve the correct position of the sample with respect to the induction coil, the upper and the lower driving shafts are controlled individually. Apart from the actuators, the coil power, the vacuum pumps, and the gas flow can be controlled from the mobile panel in the “manual mode.”

The spatial separation of the device and PC process control is necessary for the *in situ* observations during directional solidification. By activating the “auto mode,” the vacuum pumps automatically turn on, and the chamber is evacuated to $2 \cdot 10^{-5}$ mbar once the sample is placed in the device, and the door is properly closed. In a second step, the process chamber is purged with Ar. During the DS process, Ar flow is active. The PC workstation controlling the device consists of a process parameter control such as withdrawal rate, rotation speed, coil power, and movement of the positioning stage. A detailed camera view of the sample (Fig. 6) and pyrometers are incorporated into the PC controlling unit. Within the “auto mode,” the process control software saves all parameters and the corresponding changes with timestamps in a log file.

For *in situ* observations during the process, a second person is recommended to adjust the beam and run the recording of the diffraction data.

The reaction of the sample to power adjustments can be observed with the high dynamic range cameras (hema electronic GmbH, Germany, type selectorICAM weld¹⁶). One is placed to give information from below the coil, and the second one to show a view from above the coil. The cameras are sensitive to temperatures below 1000 °C, and the contrast can be adjusted for an optimal visual representation. The lenses C2514-M (KP)/Ricoh FL-CC2514-2M-1.4/25 mm from Pentax ensure a balance between clarity and details of the liquid zone. The pyrometers utilized for our device measure temperatures between 1000 °C and 3000 °C (LumaSense Technologies GmbH, Germany, type IMPAC pyrometers ISQ 5¹⁷). In the “LumaSense” software, data of both pyrometers are plotted in a temperature vs time diagram. Temperature measurement is necessary to control the process and gives information about the temperature gradient within the sample. Examples of the detailed camera view during the process are given in Figs. 6(a) and 6(b), from

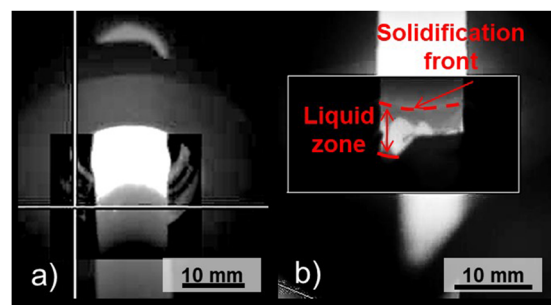


FIG. 6. Visualization of the sample from two different points of view: (a) below the coil and (b) above the coil. The inset is a so-called region of interest (ROI). In the ROI, the settings can be adjusted separately from the rest of the image.

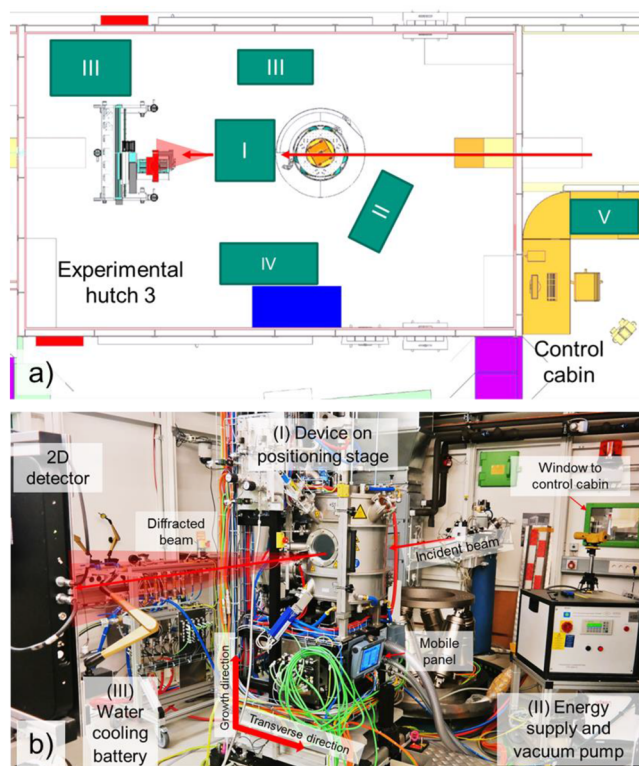


FIG. 7. (a) Ground plan of experimental hutch 3 with the installed modules of the zone melting setup: (I) the device on the positioning stage, (II) the energy supply and vacuum pump, (III) the water cooling battery and chiller, (IV) the control board, and (V) the PC workstation. (b) Illustration of the experimental setup at the P07 beamline at PETRA III, DESY, Hamburg.

below and above the coil, respectively. Both information are crucial for process control. In order to establish a stable liquid zone, sufficient power and overheating are required. When the power level is too high, depending on the liquid surface tension, an expansion of the liquid zone locally arises [Fig. 6(a)]. The surface features in Fig. 6(b) are oxide scales forming due to the oxygen in the sample. It appears brighter than the liquid beneath. Thus, these oxides visualize the movement and the overheating of the liquid zone and may serve as indicators during the process.

IV. SYSTEM INTEGRATION AT THE P07 HIGH ENERGY MATERIALS SCIENCE BEAMLINE

The modules are placed in experimental hutch 3 (EH3) at the P07 beamline at DESY in Hamburg, as illustrated in Fig. 7(a). The x-ray beam transmits the chamber from the right to the left in Figs. 7(a) and 7(b). After the interaction with the sample, the diffracted beam leaves the chamber through the larger window on the left side of the chamber and is captured with the detector placed in a certain distance from the sample. It is noteworthy that because of the crucible-free setup and the recess in the coil, the incident beam is diffracted only by the sample (without any alien reflections). This facilitates the evaluation of the diffraction data. Diffraction resulting from the windows is negligible. The on-site infrastructure, which allows beam and detector control, is used for the x-ray diffraction data acquisition.

The x-ray energy at P07 is tunable from 30 keV to 200 keV with its main optics consisting of a water-cooled double crystal monochromator in the horizontal Laue scattering geometry. The energy resolution ($\Delta E/E$) ranges from 1×10^{-3} down to 7×10^{-5} by changing the curvature of the bent Si (111) crystals in the Rowland geometry and/or inserting a channel-cut crystal. The spot size can be varied from $1 \times 1 \text{ mm}^2$ (unfocused beam) down to $2 \text{ vertical} \times 30 \text{ } \mu\text{m}^2$ horizontal (focused beam via Al compound refractive lenses) in a high-beta mode or up to $0.9 \text{ vertical} \times 6 \text{ mm}^2$ horizontal in a low-beta mode, where the beta mode is switched by changing the beta function at the undulator source position. The maximum flux currently reaches $7 \times 10^{11} \text{ ph/s}$ at 100 keV.^{18,19}

A. X-ray diffraction performance

Within the project, five material systems, as indicated in the first column of Table I, and several alloy compositions of each system were investigated. The different content of heavy elements in the systems provokes significantly different transmission behaviors. Thus, exposure times have to be adapted to the respective material (Table I). The signal-to-noise ratio obtained by maximum intensity and background for all investigated alloy systems is given in the last column of Table I. A beam size of $1 \text{ mm} \times 0.5 \text{ mm}$ was used to achieve sufficient grain statistics and conveniently short exposure times. A Perkin Elmer XRD 1621 solid-state detector with $2048 \times 2048 \text{ pixels}^2$ and a pixel size of $200 \times 200 \text{ } \mu\text{m}^2$ was used for all measurements. As seen in Table I, a photon energy between 98 keV and 103.6 keV was used, corresponding to wavelengths between

TABLE I. Experimental parameters for the investigated materials.

Material	Photon energy (keV)	Beam size (b mm \times h mm)	Exposure time (s)	Signal-to-noise ratio (a.u.)
Fe-Al ²⁰	98	1 \times 0.5	2–3	60–120
Nb-Si-Cr ²¹	98	1 \times 0.5	20–30	28–34
NiAl-Cr, Mo ²²	98–103.6	1 \times 0.5	1–12	75–225
Mo-Si-B ²³	98–103.6	1 \times 0.5	6–32	22–172
TiAl ²⁴	98–103.6	1 \times 0.5	2–6	105–135

0.126 Å and 0.119 Å. The detector was located ~ 1.9 m from the sample. The resulting maximum 2θ angle was 6° , and the step size is 0.006° . Si and CeO₂ powders were used as reference to calibrate the measurements.

V. EXAMPLES OF *IN SITU* X-RAY DIFFRACTION EXPERIMENTS DURING DIRECTIONAL SOLIDIFICATION

In the following, two examples for the *in situ* investigation of directional solidification of high melting point two-phase intermetallic materials are given. The first case focuses on the Ti–Al system or more precisely on the so-called γ -TiAl-alloys, which have been commercialized already in the investment cast, isothermally forged as well as in the additively manufactured (by EBM) form.^{25–28} DS might enable a unique combination of high creep strength and ductility,²⁹ but the decisive processing parameters are still unknown. The second case considers a high Al-containing two-phase FeAl alloy, which undergoes a high temperature eutectoid decomposition reaction upon solidification via a peritectic reaction. Here, the overarching scientific question is whether the eutectoid lamellae can be properly aligned during DS in order to also create creep-resistant microstructures at elevated temperatures. All chemical compositions mentioned in what follows are given in at. %.

A. The Ti–Al system

As mentioned above, DS is an attractive processing method for γ -TiAl-alloys because it allows us to align the constituting phases of the material.²⁹ However, the knowledge about suitable processing conditions is limited. For example, the effects of different alloy compositions on the solidification process are still not well understood. *In situ* investigations are a powerful tool to get a deep insight into the solidification of TiAl alloys. All the more, it is difficult to yield information on the solidification process from investigations at room temperature because subsequent solid-state phase transformations will mask the high-temperature situation to a significant extent.

An example of investigations on TiAl alloys is an experimental proof of the predictions for solidification,²⁴ which were made based on the “nucleation and constitutional undercooling” model of Hunziker *et al.*³⁰ If correct, a strong dependence of the type of the solidifying phase and its morphology on the G/v ratio should be found (G : temperature gradient, v : withdrawal rate). Solidification experiments with a varying withdrawal rate from some mm/h up to some hundreds mm/h were performed with different binary TiAl-alloys. Ti–45Al solidifies via the β -phase (see the phase diagram of Fig. 8). For this alloy, a change from planar to dendritic solidification with an increase in the withdrawal rate (decreasing G/v ratio) is predicted [Fig. 9(a)]. The other alloy, Ti–48Al, also changes from the planar to dendritic solidification mode with an increase in the withdrawal rate, but the solidifying phase is additionally predicted to change from an α -phase to a two-phase α/β mixture. From the diffraction ring patterns, as shown in Figs. 9(b) and 9(c), it is obvious that for Ti–48Al, the change in the solidifying phase from an α -phase to a two-phase α/β mixture with an increase in the withdrawal rate

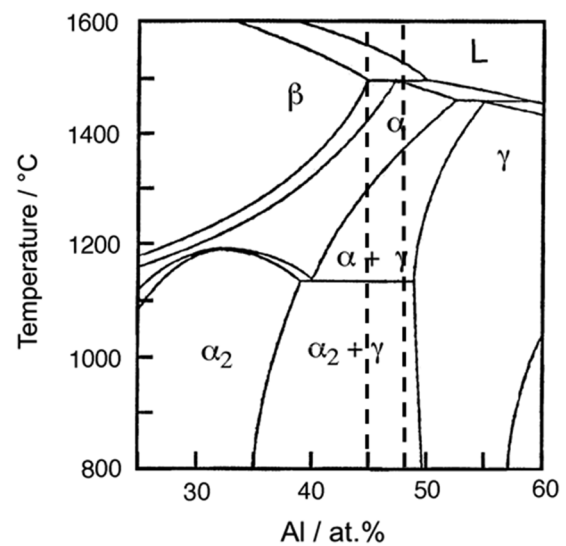


FIG. 8. Section of the equilibrium Ti–Al phase diagram.³¹ Reprinted with permission from McCullough *et al.*, *Acta Metall.* 37, 1321–1336 (1989). Copyright 1989 Elsevier.

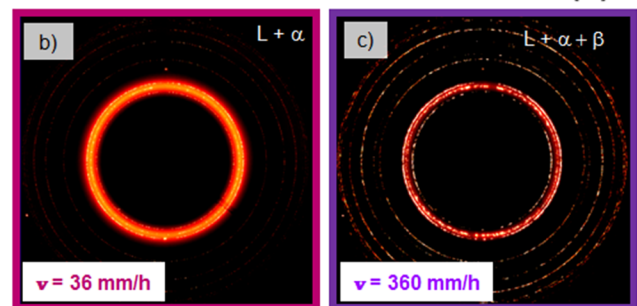
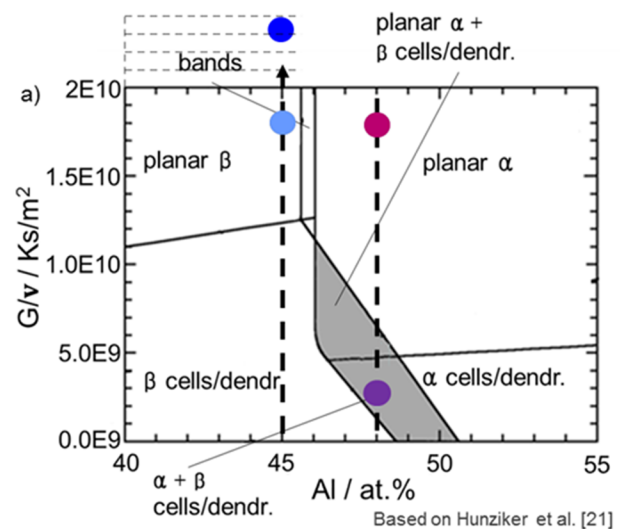


FIG. 9. (a) Predicted solidification morphology and solidifying phases in dependence on G/v and alloy composition. Resulting G/v values in the experiments are indicated by dots. Diffraction pattern of the solidification front of Ti–48Al at different withdrawal rates: (b) 36 mm/h and (c) 360 mm/h.

is experimentally verified. For a withdrawal rate of 36 mm/h, only reflections of melt (L) and α -phase were present. α - and β -phase solidify simultaneously from the melt for an increased withdrawal rate of 360 mm/h; however, the change in phase constitution occurs at a significantly lower G/v value as obtained by the model. The numerical difference might originate from improper model parameters, but this question is beyond the scope of the present work. Also other predicted effects such as a change in the solidification morphology from planar to dendritic with an increase in the withdrawal rate were confirmed in Ti-48Al and in Ti-45Al, although in the

former case, it occurred again at a lower G/v value than obtained by the model [Fig. 9(a)]. In summary, by *in situ* studies, it can be easily analyzed at which conditions certain phases and morphologies will form in TiAl alloys during solidification without being constrained by indirect conclusions as it is the case in post-process investigations.

B. The Fe–Al system

In Fe-61Al, a eutectoid decomposition of Fe_5Al_8 (Cu_5Zn_8 structure type) into FeAl (CsCl structure type) and FeAl_2 (triclinic, no other known structure of this type) occurs. The high temperature phase of Fe_5Al_8 results from a peritectic reaction, and therefore, a two-phase field must be passed in order to obtain this phase during the solidification of this specific alloy. The respective section of the equilibrium phase diagram is displayed in Fig. 10(a). The solid-state decomposition results in a lamellar microstructure being potentially promising with respect to its creep resistance in conjunction with the generally low density and very good oxidation resistance of high Al containing iron aluminides.

Diffraction patterns obtained during directional solidification of this alloy within the FlexiDS device are depicted in Figs. 10(b)–10(e). The diffraction pattern in Fig. 10(b) was obtained at the solidification front and Figs. 10(c)–10(e) at 3.5 mm, 4.5 mm, and 5.5 mm distance from the solidification front, respectively. The corresponding temperatures are indicated in Fig. 10(a). As seen in Fig. 10(c), only Fe_5Al_8 appears within the single-phase region. Retardation of the phase formation and excess FeAl_2 due to the slow peritectic reaction was not observed. The 2D diffraction patterns in Figs. 10(c)–10(e) were converted to 1D. The corresponding 1D diffraction patterns are presented in Fig. 11. Lattice parameters were found to be similar to those reported by Stein *et al.*³³ for the cast material. In contrast to expectations in Ref. 20, there is no evidence for the preferential orientation of the high temperature phase with respect to the solidification direction even though a rather large range of withdrawal rates was tested, namely, 6 mm/h–240 mm/h.

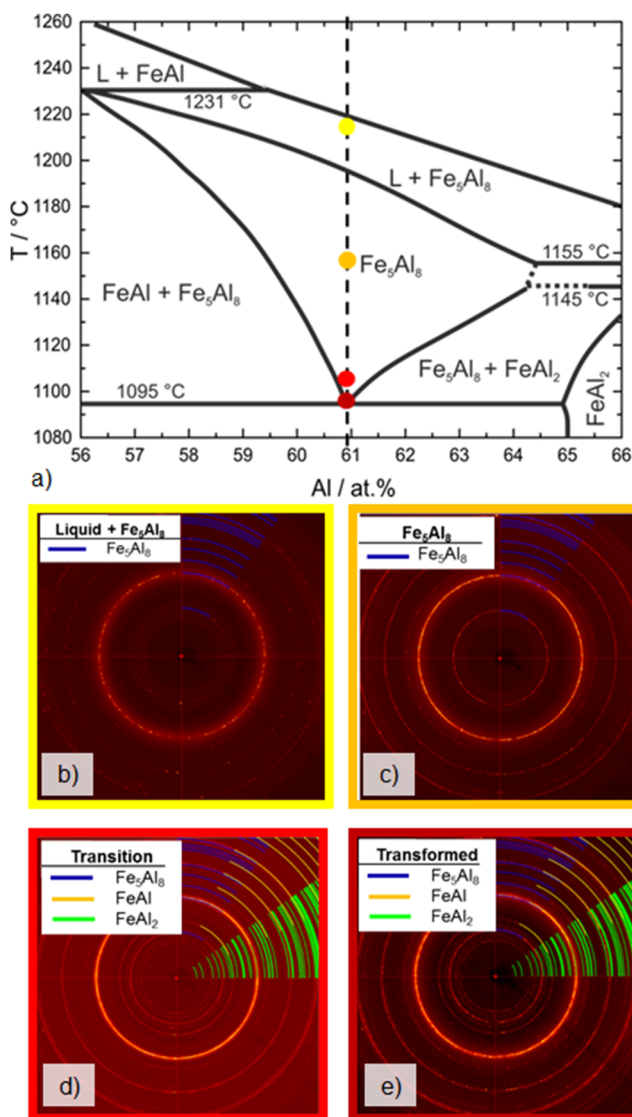


FIG. 10. (a) Section of the equilibrium Fe–Al phase diagram close to the eutectoid decomposition of Fe_5Al_8 into FeAl and FeAl_2 ³² and [(b)–(e)] diffraction patterns obtained at four different temperatures as highlighted in (a). (a) is taken from the work of Li *et al.*, *J. Phase Equilib. Diffus.* **37**, 162–173 (2016). Copyright 2016 Author(s) licensed under a Creative Commons Attribution 4.0 license.

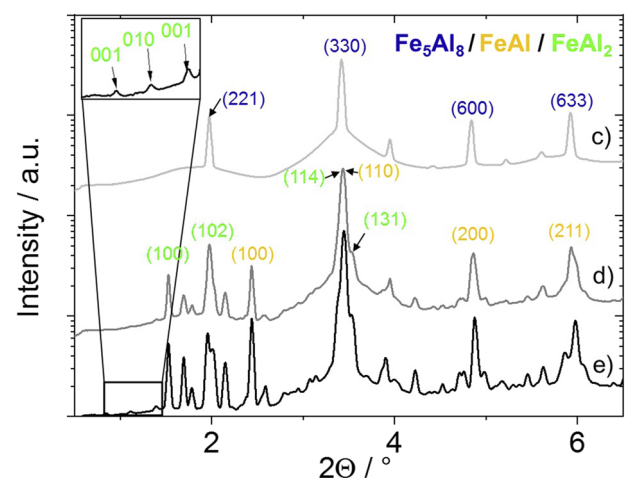


FIG. 11. Diffraction patterns from Figs. 10(c)–10(e) converted to 1D diffraction patterns.

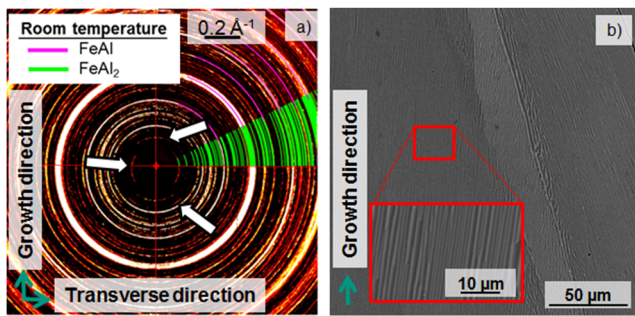


FIG. 12. (a) Diffraction pattern of Fe-61Al at room temperature subsequent to directional solidification at 120 mm/h. Slight crystallographic texture is obtained for FeAl₂ indicated by inhomogeneous intensity distribution along the (001), (010), and (011) diffraction rings highlighted with arrows. (b) Scanning electron micrograph (backscatter electron imaging) of a longitudinal section of the directionally solidified material (bright phase is FeAl, and dark phase is FeAl₂).

Nevertheless, columnar Fe₅Al₈ grains form at high withdrawal rates, which results in columnar eutectoid colonies after completion of the eutectoid reaction. For withdrawal rates higher than 120 mm/h, inhomogeneous intensity distributions for the (001), (010), and (011) diffraction rings of FeAl₂ indicative of a crystallographic texture are observed in Fig. 12(a). Indeed, a majority of the lamellae in the eutectoid microstructure are aligned with respect to the temperature gradient, as seen in Fig. 12(b). For a single orientation of Fe₅Al₈, 12 different orientation variants of the lamellae could be expected based on the distinct orientation relationship of FeAl and FeAl₂.²⁰ Obviously, high withdrawal rates lead to a variant selection of the colonies in the temperature gradient during the eutectoid reaction even though the parent phase does not exhibit preferential orientation. Without the application of *in situ* observation of the solidification and cooling process, this information would not have been accessible.

VI. SUMMARY

We introduced the new state-of-the-art FlexiDS device for the time-resolved *in situ* investigation of directional solidification processes using high-energy synchrotron radiation. The system is a valuable addition to the infrastructure of PETRA III at DESY, being specifically designed for the use at the P07 HEMS beamline. The apparatus is capable of investigating liquid–solid regions, transformations, and decompositions in various structural intermetallic materials. Moreover, we could show the wide operation range by means of sample geometry, densities, and alloy compositions as well as a process parameter such as a withdrawal rate. Even during experiments that exceed a liquidus temperature of 2000 °C, the device operated stably and a satisfactory diffraction pattern was obtained. Trial tests of time-resolved processes of TiAl and FeAl alloys were presented in this work. Further detailed experimental results are forthcoming and will be published elsewhere, for instance, Ref. 22. Not being installed at the beamline, the FlexiDS device is available at the Helmholtz-Zentrum Geesthacht. Possible trial tests on new alloys can be performed there without using high-energy synchrotron radiation in order to get used to the device. We

strongly welcome and encourage collaboration from the materials science research community in order to maximize the potential of this unique *in situ* directional solidification device for improving understanding of fundamental solidification processes.

ACKNOWLEDGMENTS

This research was financially supported by the German Federal Ministry of Education and Research (BMBF) program “FlexiDS” (Grant No. 05K2016).

The authors gratefully acknowledge S. Huisl and M. Gleichmann from the Systec Group and W. Ripp from ITG for the manufacturing and implementation of the FlexiDS device and the close cooperation.

The authors are grateful to D. Matthiessen for the helpful experimental support.

DATA AVAILABILITY

The data that support the findings of this study are available from the corresponding author upon reasonable request.

REFERENCES

- 1 R. C. Reed, *The Superalloys: Fundamentals and Applications* (Cambridge University Press, Cambridge, 2006).
- 2 T. Haenschke, A. Gali, M. Heilmaier, M. Krüger, H. Bei, and E. P. George, “Synthesis and characterization of lamellar and fibre-reinforced NiAl-Mo and NiAl-Cr,” *J. Phys.: Conf. Ser.* **240**, 012063 (2010).
- 3 H. Bei and E. P. George, “Microstructures and mechanical properties of a directionally solidified NiAl-Mo eutectic alloy,” *Acta Mater.* **53**, 69–77 (2005).
- 4 H. E. Cline, J. L. Walter, E. Lifshin, and R. R. Russell, “Structures, faults, and the rod-plate transition in eutectics,” *Metall. Trans.* **2**, 189–194 (1971).
- 5 H. E. Cline and J. L. Walter, “The effect of alloy additions on the rod-plate transition in the eutectic NiAl-Cr,” *Metall. Trans.* **1**, 2907–2917 (1971).
- 6 G. Frommeyer, R. Rablbauer, and H. J. Schäfer, “Elastic properties of B2-ordered NiAl and NiAl-X (Cr, Mo, W) alloys,” *Intermetallics* **18**, 299–305 (2010).
- 7 A. Misra, R. Gibala, and R. D. Noebe, “Optimization of toughness and strength in multiphase intermetallics,” *Intermetallics* **9**, 971–978 (2001).
- 8 C. Seemüller, M. Heilmaier, T. Haenschke, H. Bei, A. Dlouhy, and E. P. George, “Influence of fiber alignment on creep in directionally solidified NiAl-10Mo *in situ* composites,” *Intermetallics* **35**, 110–115 (2013).
- 9 D. R. Johnson, X. F. Chen, B. F. Oliver, R. D. Noebe, and J. D. Whittenberger, “Processing and mechanical properties of *in situ* composites from the NiAl-Cr and the NiAl-(Cr,Mo) eutectic systems,” *Intermetallics* **3**, 99–113 (1995).
- 10 J. D. Whittenberger, S. V. Raj, I. E. Locci, and J. A. Salem, “Effect of growth rate on elevated temperature plastic flow and room temperature fracture toughness of directionally solidified NiAl-31Cr-3Mo,” *Intermetallics* **7**, 1159–1168 (1999).
- 11 N. Shevchenko, S. Boden, G. Gerbeth, and S. Eckert, “Chimney formation in solidifying Ga-25 wt pct In alloys under the influence of thermosolutal melt convection,” *Metall. Mater. Trans. A* **44**, 3797–3808 (2013).
- 12 N. Shevchenko, O. Roshchupkina, O. Sokolova, and S. Eckert, “The effect of natural and forced melt convection on dendritic solidification in Ga-In alloys,” *J. Cryst. Growth* **417**, 1–8 (2015).
- 13 A. Saad, C.-A. Gandin, M. Bellet, N. Shevchenko, and S. Eckert, “Simulation of channel segregation during directional solidification of In-75 wt pct Ga. Qualitative comparison with *in situ* observations,” *Metall. Mater. Trans. A* **46**, 4886–4897 (2015).
- 14 See <https://www.systec-fertigungstechnik.de/produkte/maschinen-und-anlagenbau.html> for SYSTEC Fertigungstechnik GmbH & Co.KG, Products; retrieved 2 June 2020.

- ¹⁵See <https://www.itg-induktion.de/en/home> for iTG Induktionsanlagen GmbH; retrieved from 02 June 2020.
- ¹⁶See <https://www.hema.de/en/services/products/seelector-icam-weld> for Hema Electronic, Products; retrieved 2 June 2020.
- ¹⁷See <https://www.advancedenergy.com/products/temperature-measurement/thermal-measurement-optical-pyrometers-power-controllers/metal-applications-pyrometers/impac-is-5-iga-5/> for Advanced Energy, Products; retrieved 2 June 2020.
- ¹⁸N. Schell, A. King, F. Beckmann, T. Fischer, M. Müller, and A. Schreyer, “The high energy materials science beamline (HEMS) at PETRA III,” *Mater. Sci. Forum* **772**, 57–61 (2013).
- ¹⁹N. Schell, The High Energy Materials Science Beamline of Helmholtz-Zentrum Geesthacht (HZG) and DESY, 2020; retrieved from http://photon-science.desy.de/facilities/petra_iii/beamlines/p07_high_energy_materials_science/index_eng.html.
- ²⁰A. Scherf, A. Kauffmann, S. Kauffmann-Weiss, T. Scherer, X. Li, F. Stein, and M. Heilmaier, “Orientation relationship of eutectoid FeAl and FeAl₂,” *J. Appl. Crystallogr.* **49**, 442–449 (2016).
- ²¹F. Gang, A. Kauffmann, and M. Heilmaier, *Metall. Mater. Trans. A* **49**, 763–771 (2018).
- ²²C. Gombola, A. Kauffmann, G. Geramifard, M. Blankenburg, and M. Heilmaier, “Microstructural investigations of novel high temperature alloys based on NiAl-(Cr,Mo),” *Metals* **10**, 961 (2020).
- ²³G. Hasemann, S. Ida, L. Zhu, T. Iizawa, K. Yoshimi, and M. Krüger, “Experimental assessment of the microstructure evolution and liquidus projection in the Mo-rich Mo-Si-B system,” *Mater. Des.* **185**, 108233 (2020).
- ²⁴M. Oehring, V. Küstner, F. Appel, and U. Lorenz, “Analysis of the solidification microstructure of multi-component γ -TiAl alloys,” *Mater. Sci. Forum* **539-543**, 1475–1480 (2007).
- ²⁵B. P. Bewlay, S. Nag, A. Suzuki, and M. J. Weimer, “TiAl alloys in commercial aircraft engines,” *Mater. High Temp.* **33**, 549–559 (2016).
- ²⁶M. Todai, T. Nakano, T. Liu, H. Y. Yasuda, K. Hagihara, K. Cho, M. Ueda, and M. Takeyama, “Effect of building direction on the microstructure and tensile properties of Ti-48Al-2Cr-2Nb alloy additively manufactured by electron beam melting,” *Addit. Manuf.* **13**, 61–70 (2017).
- ²⁷M. Thomas, T. Malot, P. Aubry, C. Colin, T. Vilaro, and P. Bertrand, “The prospects for additive manufacturing of bulk TiAl alloy,” *Mater. High Temp.* **33**, 571–577 (2016).
- ²⁸S. Mayer, P. Erdelyi, F. D. Fischer, D. Holec, M. Kasthuber, T. Klein, and H. Clemens, “Intermetallic β -solidifying γ -TiAl based alloys – from fundamental research to application,” *Adv. Eng. Mater.* **19**, 1600735 (2017).
- ²⁹M. Yamguchi, H. Inui, and K. Ito, “High-temperature structural intermetallics,” *Acta Mater.* **48**, 307–322 (2000).
- ³⁰O. Hunziker, M. Vandyoussefi, and W. Kurz, *Acta Mater.* **46**, 6325–6336 (1998).
- ³¹C. McCullough, J. J. Valencia, C. G. Levi, and R. Mehrabian, *Acta Metall.* **37**, 1321–1336 (1989).
- ³²X. Li, A. Scherf, M. Heilmaier, and F. Stein, “The Al-rich part of the Fe-Al phase diagram,” *J. Phase Equilib. Diffus.* **37**, 162–173 (2016).
- ³³F. Stein, S. C. Vogel, M. Eumann, and M. Palm, “Determination of the crystal structure of the ϵ phase in the Fe-Al system by high-temperature neutron diffraction,” *Intermetallics* **18**, 150–156 (2010).